Artical ID:1006-3471(2012)05-0457-15

The Oxidation of Hydrogen Peroxide on Nanostructured Rhodium Microelectrodes

Philip N. Bartlett*, Thomas F. Esterle[1]
(*Chemistry, University of Southampton, Southampton, SO17 1BJ, UK*)

Abstract: Mesoporous Rh films were deposited onto platinum microelectrodes from the H_1 lyotropic liquid crystalline phase of $C_{12}EO_8$ (octaethyleneglycol monododecyl ether). The electrodes show well defined voltammetry for the oxidation and the reduction of hydrogen peroxide at low concentrations (<10 mmol·L^{-1}) with excellent stability for operation at neutral pH. Based on the hysteresis in the current and the potential dependence the oxidation of hydrogen peroxide occurs through a CEE mechanism involving $Rh(OH)_3$ on the mesoporous Rh electrode surface. At higher hydrogen peroxide concentrations the current reaches a plateau that is due to either saturation of the binding sites for hydrogen peroxide or limitation of the reaction due to acidification of the solution within the pores. For the thin films (below 200 nm) the hydrogen peroxide calibration curves we fitted to a one dimensional model for diffusion and reaction within the pores.

Key words: hydrogen peroxide; rhodium; microelectrode; nanoporous; lyotropic liquid crystal; templated electrodeposition

CLC Number: O646 **Document Code:** A

1 Introduction

Mesoporous metal films with regular nanoporous architectures between about 2 and 10 nm can be electrodeposited from hexagonal lyotropic liquid crystalline phases[1]. They represent an interesting type of high surface area metallic structure in which the surface is concave and strongly curved in contrast to the much more widely studied convex surfaces of nanoparticulate systems. One of the potential practical applications of mesoporous metal films is for the detection of hydrogen peroxide over a wide range of concentrations[2]. Hydrogen peroxide is of interest in many fields[3], in industrial processes[4], for example in the food industry[5], as well as in waste water treatment[6]. In particular, many investigations have been undertaken of the amperometric detection of hydrogen peroxide for biosensing applications[7]. Relevant analytical hydrogen peroxide concentrations range from micromolar for *in vivo* applications to millimolar for bleaching and even molar in the field of water treatment.

The accurate amperometric measurement of hydrogen peroxide has been a difficult task since the reactions at the electrode are irreversible and the voltammograms are often irreproducible. Different electrode materials have been used to monitor hydrogen peroxide, including carbon fibres[8], glassy carbon[9], and platinum[10]. However, in many cases the electrodes show poor stability and the amperometric response becomes non-linear at high hydrogen peroxide concentrations.

Solutions have been put forward to overcome the irreproducibility and instability of the responses such as the modification of the electrode surface with enzymes (horseradish peroxidise[11] and others[12-13]) or Prussian Blue[14]. Enzyme based biosensors

Received: 2012-06-14, Revised: 2012-08-01 *Corresponding author, E-mail: pnb@soton.ac.uk
[1]Now at: Department d'Enginyeria Quimica, Universitat Rovira i Virgili, Avinguda Paĭsos Catalans 26, 43007 Tarragona, Spain
This work was supported by the EPSRC Grant EP/E0473X/1.

have shown a high sensitivity (1.5 A·mol^{-1}·L·cm^{-2}) and very low detection limits (10 nmol·L^{-1})[15], however in this case the upper limit does not go beyond 12 mmol·L^{-1} [16]. Another disadvantage was that the stability of the Prussian-Blue based sensor decreased with repeated use[16].

The oxidation of hydrogen peroxide has been studied on platinum and platinum/iridium electrodes and a decrease in the response was observed above 1 mmol·L^{-1}, this was attributed to the saturation of oxygen and hydrogen peroxide on the platinum catalytic sites[17]. Gorton came to the same conclusion in his study of the mechanism for hydrogen peroxide oxidation on high surface palladium electrodes[18]. Johnston et al. proposed a surface binding site model for hydrogen peroxide oxidation on palladium assuming that the reaction obeys a form of Michaelis-Menten kinetics[19]. An identical surface binding site model was then adapted by Hall et al. for hydrogen peroxide oxidation on Pt electrodes[20-24]. According to a series of papers from Hall et al.[20-24], the oxidation current for hydrogen peroxide oxidation is under mixed kinetic and diffusion control and occurs through a CEE mechanism (chemical reaction step by two sequential electrochemical steps) in which hydrogen peroxide is adsorbed and then oxidised at the oxide coated metal surface in a chemical step which is followed by the electrochemical reformation of the surface oxide. The availability of Pt oxide sites is then a limiting factor in the reaction at high hydrogen peroxide concentrations and this results in the saturation of the response. This mechanism also accounts for the ready poisoning of the reaction since the catalytic sites can be blocked by other species from solution.

Microdisc electrodes are attractive for amperometric analytical measurements because under mass transport limited conditions they attain a steady state in which the limiting current is proportional to concentration. However, this advantage is not readily realised in the case of hydrogen peroxide because of the CEE mechanism. A way to overcome this problem is to increase the electroactive surface area whilst maintaining the diffusion properties of the microelectrodes and this can be achieved by coating the microelectrode with a high surface area mesoporous metal film, for example of platinum, by deposition from the hexagonal lyotropic liquid crystalline phase as described by Elliott et al. [25]. Hydrogen peroxide electrochemistry has been investigated on H_1e mesoporous Pt films (where H_1e denotes the film electroplated from the H_1 lyotropic liquid crystalline phase) deposited on platinum microelectrodes [2] and the steady-state response was found to be stable over a wide linear range. In a separate paper, Han et al. used hydrogen peroxide detection on an H_1e mesoporous Pt film as part of a glutamate microsensor[26].

In the present work we have investigated the use of H_1e rhodium films for hydrogen peroxide oxidation. Rhodium has the advantage that the oxide is formed at lower potential than for platinum or palladium and this should allow the use of lower potentials for hydrogen peroxide detection. In turn this offers the potential advantage of reduced interferences from other species such as ascorbate, acetamidophenol or uric acid when using the electrode in biological samples at neutral pH. Rivas et al. have used rhodinized glassy carbon for hydrogen peroxide oxidation in glucose biosensors [27-28]. Here we present results for hydrogen peroxide oxidation at H_1e Rh coated microelectrodes as a function of film thickness in pH 7 phosphate buffer and we analyse the results in terms of a mechanism which combines mass transport in the mesoporous film with reaction at the surface of the nanopores through the CEE mechanism.

2 Experimental

Platinum microdiscs were made by sealing platinum wires of the appropriate diameter into glass and were polished with a slurry of 0.3 μm alumina (Buehler) to obtain a fine mirror finish on a Buehler microcloth. The microelectrodes were then cleaned by cycling in sulphuric acid. All solutions were prepared using water from a Whatman Still and RO 50 water purification system.

The polished platinum disc microelectrodes were modified by the electrodeposition of a mesoporous rhodium film using a plating mixture prepared from an aqueous solution containing 47wt.% $C_{12}EO_8$ (octaethyleneglycol monododecyl ether, 98% purity, Fluka), 12wt.% $RhCl_3$ (99.9% purity, Sigma-Aldrich), 39wt.% deionised water and 2wt.% n-heptane (99% purity, Sigma-Aldrich). Heptane was added to the composition to obtain the hexagonal phase as reported by Bartlett and Marwan in their work using $C_{16}EO_8$ as the surfactant[29]. The metal film is obtained by the electroreduction of the metal from the hexagonal lyotropic liquid crystalline phase. The exact phase was identified by polarised optical microscopy (Olympus BH-2 polarized light microscope equipped with a Linkam TMS90 heating/cooling stage and a control unit). Electrodeposition of the H₁e rhodium film was carried out at -0.2 V vs. SCE (saturared calomel electrodes) until the required charge had been passed. The electrode was then soaked in iso-propanol (HPLC, Rathburn) and then in water overnight to remove the plating mixture from the electrode surface. The thickness of the film was estimated from the deposition charge assuming 100% Faradaic efficiency and taking the idealized hexagonal structure for the mesoporous film, assuming 4.5 nm pore diameter with 6.5 nm centre to centre spacing. This gives a value for the thickness per unit charge, σ, of 289 cm·C^{-1} for deposition on a 25 μm diameter microdisc.

Cyclic voltammetry was performed to remove any residual plating mixture from the pores by cycling between -0.70 and 0.85 V vs. SMSE (saturated mercurous sulphate electrode) at 200 mV·s^{-1} in 1 mol·L^{-1} sulphuric acid until a stable cyclic voltammogram was obtained (after 20 and 30 cycles). The electrodes were kept in deionised water at room temperature when not in use.

Cyclic voltammetry and electrochemical depositions were performed using an EG&G model 263A potentiostat/galvanostat. Electrochemical impedance spectroscopy was performed using an Autolab PGSTAT30. SEM images of the microelectrodes were obtained with a Philips XL30 ESEM. Transmission electron microscopy of the H₁e Rh was obtained using a JOEL 3010 TEM. The samples were prepared by scraping particles of the electrodeposit from the surface of an evaporated gold electrode onto a 300 mesh carbon TEM grid (Agar) using a scalpel blade. Small angle XRD was performed using a Bruker D5000 using 0.154 nm Cu-K_α radiation, scanning from 0.5° to 6° at 12°·min^{-1}.

Hydrogen peroxide solutions were standardised by iodometric titration according to the method of Vogel[30] and solutions were diluted as required in 0.1 mol·L^{-1} pH 7 sodium phosphate buffer or water. Calibration curves for hydrogen peroxide were obtained in a water jacketed cell thermostated at 25 °C with a platinum gauze counter electrode. The potential at the working electrode (5, 10, 25 and 50 μm in diameter for microelectrodes and 0.5 cm for the RDE) was held at 0 V vs. SMSE in 0.1 mol·L^{-1} pH 7 sodium phosphate buffer. The background current was recorded 20 min before adding 20 aliquots of H_2O_2. The solution was stirred during addition using a magnetic stirrer. After addition of H_2O_2 and stirring for 1 min, the stirring was stopped and measurement was made for 2 ~ 3 min (when the current became stable) before the next addition of H_2O_2. Rotating disc electrode measurements were carried out using an H₁e Rh coated Pt RDE (Pine Research Instrumentation AFE3T-50PT electrode and AF CPRB E rotator).

3 Results and Discussion

3.1 Characterisation of Mesoporous Rhodium Films

The mesoporous rhodium films were characterised by voltammetry, TEM and small angle X-ray diffraction. Fig. 1 shows the cyclic voltammogram of a H₁e mesoporous Rh coated microelectrode in 1 mol·L^{-1} sulphuric acid.

The characteristics of the cyclic voltammogram for H_1 mesoporous Rh in sulphuric acid are the same as those of polycrystalline rhodium[31]. According to Jerkiewicz et al.[31-32], different oxide films on Rh

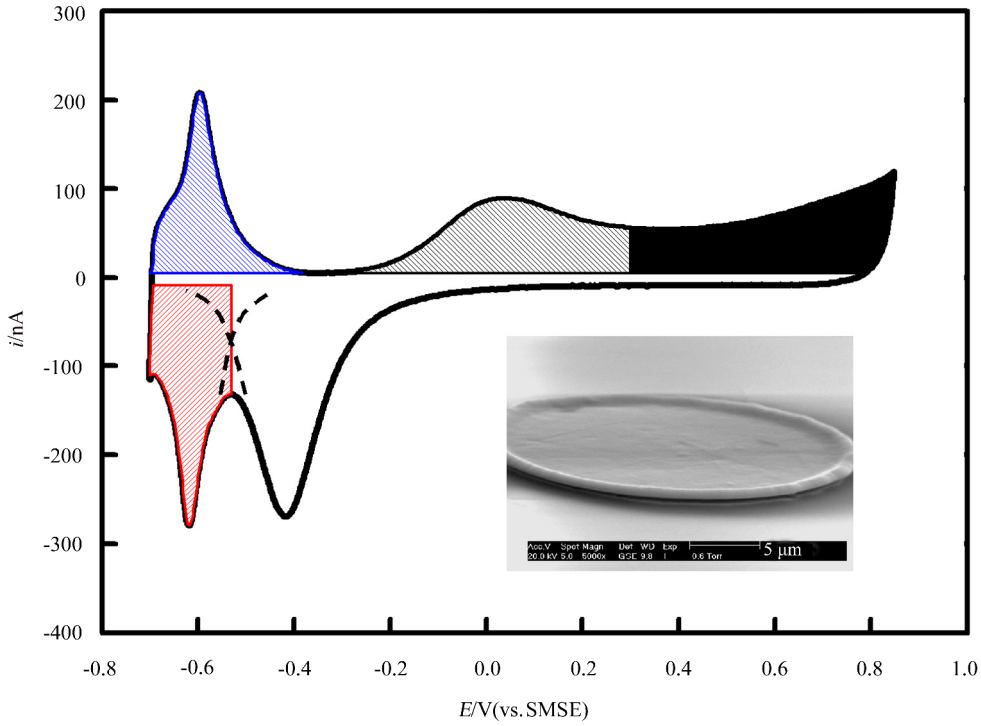

Fig. 1 Cyclic voltammogram of an H_1e mesoporous Rh film electrodeposited onto a platinum disc microelectrode (25 μm in diameter, 8.68 μC deposition charge) recorded at 50 mV·s^{-1} in 1 mol·L^{-1} sulphuric acid. The solution was deaerated by purging with argon for at least 20 min prior to the measurements. The crossed blue area corresponds to hydrogen desorption and the red area to hydrogen adsorption and a part of the oxide stripping peak. The dashed lines correspond to the continuity of the peaks and give rise to the peak overlapping. The grey area corresponds to the formation of Rh(OH) and the black area corresponds to the formation of $Rh(OH)_3$ (assignments based on the work of Jerkiewicz et al.[31-32]). The inset shows an SEM image of a coated electrode (25 μm diameter, 8.68 μC for the deposition charge) at a tilt angle of 70°.

grow with increasing potential on the anodic sweep. The first oxide formation on Rh starts at -0.2 V vs. SMSE and involves the electrochemisorption of one monolayer of OH resulting in the formation of Rh (OH) species (cross hatched area in Fig. 1). At about 0.3 V vs. SMSE further oxidation and the formation of $Rh(OH)_3$ species (shaded area in Fig. 1) occurs. These oxide species were identified for Rh electrodes in a study by Peuckert using combined X-ray Photoelectron Spectroscopy (XPS) measurements and voltammetry[33]. Simultaneously with the electrosorption of OH on the rhodium surface, a place exchange occurs between rhodium atoms and the adsorbed OH species leading to a reorganisation of the rhodium superficial layer[34]. At higher anodic potentials RhO(OH) can form but under the present conditions we believe we only form $Rh(OH)_3$ because there is only one stripping oxide peak in the cyclic voltammogram[31-32].

The hydrogen peaks for the H_1e mesoporous Rh film in the potential range -0.4 to -0.7 V are similar to those reported for polycrystalline Rh electrodes, with a peak for hydrogen adsorption (red hatching in Fig. 1) at -0.62 V on the cathodic sweep and for hydrogen desorption at -0.6 V vs. SMSE on the anodic sweep (blue hatching in Fig. 1). The surface area of rhodium electrodes can be calculated from the area of the oxide formation peaks by using a conversion factor of 660 μC·cm^{-2} or from the area under the hydrogen desorption peak using a conversion factor of 221 μC·cm^{-2}[31]. The conversion factor of 660 μC·cm^{-2} corresponds to the experimental-conditions in which the scan rate was 50 mV·s^{-1}, the electrolyte was 0.5 mol·L^{-1} H_2SO_4 and the anodic

potential limit was 1.3 V vs. NHE[31]. Using either the hydrogen adsorption peak or the oxide stripping peak to determine the surface area is problematic because the peaks overlap. For this reason, the surface area was calculated from the hydrogen desorption peak (after subtracting the contribution from double layer charging). The resulting calculated surface area is 380±50 times the geometric area of the electrode, consistent with the regular, highly porous structure expected for the H_1e film.

TEM, Fig. 2, confirms the regular nanoporous structure of the H_1e Rh films. Pores can be observed on the thinnest edges of the particle with rows of pores running through the metal arranged in a hexagonal array. Based on the TEM, the pore size was estimated to be 4.5±0.2 nm with a wall thickness of ~ 2.0 nm. These values are similar to those reported in earlier studies of mesoporous Rh[29] and also in studies of other mesoporous metals electrodeposited from the hexagonal lyotropic liquid crystalline phase using $C_{12}EO_8$ and heptane[1]. Small angle XRD (supplementary information) of the material shows a well resolved peak at 2θ of 2.24° corresponding to a (100) lattice spacing with a pore size of 4±1 nm.

The results of the voltammetry in acid, TEM and small angle XRD all confirm the successful electrodeposition of the nanostructured H_1e Rhodium films.

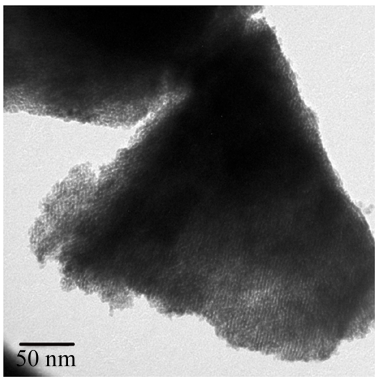

Fig. 2 TEM image of an H_1e Rh sample electrodeposited on a gold coated glass slide from a mixture of 12 wt% RhC_{13}, 47 wt% $C_{12}EO_8$, 39 wt% water and 2 wt% heptane at -0.2 V vs. SCE.

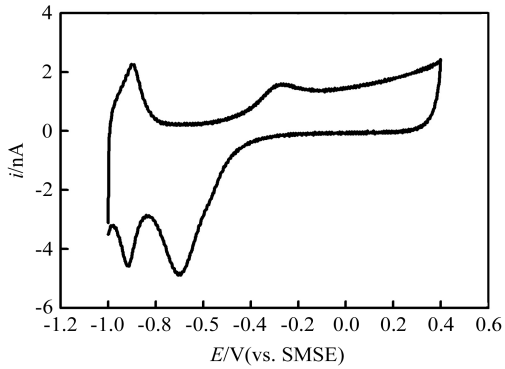

Fig. 3 Cyclic voltammogram of a H_1e Rh film deposited on a platinum disc microelectrode (25 μm diameter, 8.68 μC deposition charge) in 0.1 mol·L^{-1} pH 7 phosphate buffer recorded at 2 mV·s^{-1}. The solution was deaerated by purging with argon for at least 20 min prior to the measurements.

3.2 Voltammetry of Mesoporous Rhodium in Phosphate Buffer

Fig. 3 shows a cyclic voltammogram for an H_1e Rh coated microelectrode in pH 7 phosphate buffer.

The voltammetry is very similar to that in sulphuric acid (compared to Fig. 1) with the same surface processes occurring. The major difference is that the potentials are all shifted cathodically by 300 mV, there is also some broadening of the peaks. This shift is somewhat less than the predicted shift of 413 mV calculated on the basis of a shift of 59 mV per pH unit for processes involving equal numbers of protons and electrons and assuming a pH of 0 for 1 mol·L^{-1} sulphuric acid. This probably reflects a local pH change within the pores during cycling, which is consistent with observation that the peaks are somewhat broader even though the scan rate is much slower. The similarity in voltammetry confirms that the same surface oxides are involved in neutral and acid solution.

3.3 Voltammetry of Hydrogen Peroxide on H_1e Rh at Neutral pH

Fig. 4 shows a cyclic voltammogram for an H_1e Rh coated microelectrode with 5 mmol·L^{-1} hydrogen peroxide in 0.1 mol·L^{-1} pH 7 sodium phosphate buffer.

It is notable that hydrogen peroxide oxidation occurs at the same potential as the oxidation of the Rh surface to $Rh(OH)_3$ in pH 7 phosphate buffer (compared Figs. 3 and 4) and the hysteresis in the hydrogen peroxide voltammetry corresponds to the hysteresis in the formation of $Rh(OH)_3$ from Rh(OH) and the oxide stripping. The oxidation and reduction of hydrogen peroxide depend on the rhodium surface state: if the rhodium surface is in the oxidised $Rh(OH)_3$ state it can catalyse hydrogen peroxide oxidation; on the other hand, the oxide free rhodium surface catalyses the hydrogen peroxide reduction as shown by the limiting reduction current at cathodic potential. It is interesting to note that the potential of zero current in Fig. 4 corresponds to the mass transport limited disproportionation of hydrogen peroxide at the Rh surface:

$$2H_2O_2 \rightarrow 2H_2O + O_2 \quad (1)$$

This same behaviour is seen on platinum but occurs around 0.2 to 0.3 V more cathodic. For a recent discussion of this reaction on Pt in the context of the oxygen reduction reaction see the recent work of Katsounaros et al[35].

For potentials negative of -0.6 V, three peaks are observed when H_2O_2 reduction occurs: one on the anodic sweep (I) and two on the cathodic sweep (II and III). These peaks can be identified by reference to the voltammetry in phosphate buffer shown in Fig. 3; the two peaks (I) and (II) at ~ -0.9 V correspond to hydrogen desorption/adsorption, the cathodic peak (III) at ~ -0.7 V corresponds to the oxide stripping peak. The charge under peak (I) corresponds to 60 % of the charge measured for hydrogen desorption in sulphuric acid.

Using the microdisc equation

$$i_L = 4nFD[H_2O_2]_{bulk}a \quad (2)$$

where n is the number of electrons transferred, F is the Faraday, $[H_2O_2]_{bulk}$ is the concentration of the hydrogen peroxide, D its diffusion coefficient and a the radius of the microdisc, we can determine the diffusion coefficient for hydrogen peroxide. The limiting current was recorded for 5 mmol·L^{-1} H_2O_2 in 0.1 mol·L^{-1} pH 7 phosphate buffer H_1e Rh coated microelectrodes with diameters of 5, 10, 25 and 50 μm, Fig. 5. In each case the diameter of the microelectrode was verified by SEM before and after deposition in case of any overgrowth of the film. From the slope (assuming n = 2) we obtain a value for D of $1.48\times10^{-5} \pm 0.08$ $cm^2\cdot s^{-1}$. This is in good agreement with the values reported by other authors under similar conditions: $1.43\times10^{-5} \pm 0.08$ $cm^2\cdot s^{-1}$ van Stroe-Biezen et al.[36] in 0.1 mol·L^{-1} pH 6.7 sodi-

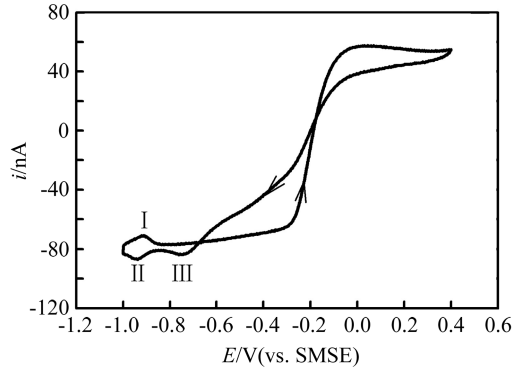

Fig. 4 Cyclic voltammogram of an H_1e Rh film on a platinum disc microelectrode (25 μm diameter, 8.68 μC deposition charge) in 5 mmol·L^{-1} H_2O_2, 0.1 mol·L^{-1} pH 7 phosphate buffer recorded at 2 mV·s^{-1}. The solution was deaerated by purging with argon for at least 20 min prior to the measurements. The arrows indicate the direction of the cycle.

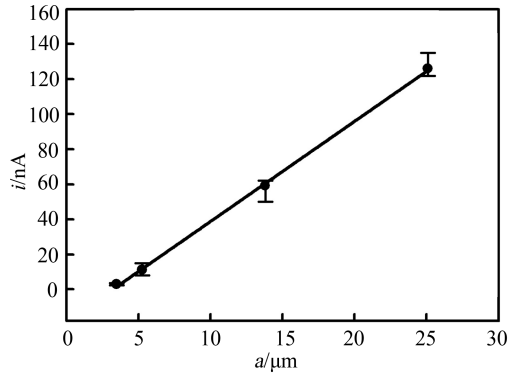

Fig. 5 Limiting currents of hydrogen peroxide oxidation (corrected for double layer charging) recorded for different radii of microdisc electrodes for 5 mmol·L^{-1} H_2O_2 in 0.1 mol·L^{-1} pH 7 sodium phosphate buffer. The solid line represents a linear fit of the data points. The error bars correspond to measurements from three different voltammograms.

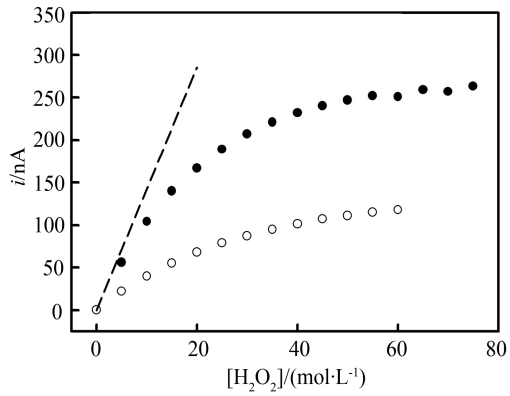

Fig. 6 Calibration curves recorded at 0.0 V vs. SMSE for hydrogen peroxide oxidation at a polished 25 μm Pt microelectrode (○) and an H_1e Rh coated 25 μm microelectrode (deposition charge 5.52 μC) (●) in 0.1 mol·L^{-1} pH 7 phosphate buffer at 25 ℃. The electrode was held at 0 V vs. SMSE for 20 min before the addition of aliquots of hydrogen peroxide. Calculated mass transport limited current assuming n = 2 and D = 1.48×10^{-5} cm^2·s^{-1} (dashed line).

um phosphate buffer by Koutecky-Levich; 1.46×10^{-5} cm^2·s^{-1} Evans et al.[2] in 0.1 mol·L^{-1} pH 7 sodium phosphate buffer by chronoamperometry.

Calibration plots were obtained by adding aliquots of hydrogen peroxide in 0.1 mol·L^{-1} phosphate buffer. Fig. 6 compares the calibration curve obtained for a polished Pt microelectrode with a calibration curve recorded for an H_1e Rh coated microelectrode of the same diameter.

From Fig. 6 we can see that the current for the polished Pt microelectrode is significantly lower than that on the H_1e Rh electrode and, even at low hydrogen peroxide concentrations it does not approach the mass transport limited value; this is because of the kinetic limitation of the reaction on the Pt surface[17]. On the H_1e Rh coated microelectrode the current is linear in hydrogen peroxide concentration for low concentrations (< 10 mmol·L^{-1}, data not shown) and shows a good agreement with the mass transport limited value. At higher concentrations the current starts to deviate and reaches a plateau.

3.4 The Mechanism for Hydrogen Peroxide Oxidation

Hall et al. in a series of papers describe a CEE mechanism for the oxidation of hydrogen peroxide on Pt based on rotating disc measurements[20-24]. The results in Figs. 4 and 6 are consistent with a similar mechanism, involving the surface $Rh(OH)_3$ oxide species, for the reaction on rhodium.

$$H_2O_2+Rh(OH)_3 \overset{K_M}{\longleftrightarrow} Rh(OH)_3\cdot H_2O_2 \quad (3)$$

$$Rh(OH)_3\cdot H_2O_2 \xrightarrow{k_{cat}} Rh(OH)+2H_2O+O_2 \quad (4)$$

$$Rh(OH)+2H_2O \xrightarrow{k'_E} Rh(OH)_3+2H^++2e \quad (5)$$

where K_M is the equilibrium constant for H_2O_2 adsorption and K_{cat} the rate constant for the oxidation of the adsorbed H_2O_2.

The H_1e Rh film comprises an hexagonal array of ~ 4 nm diameter high aspect ratio cylindrical pores separated by walls ~ 2 nm thick. For this geometry we can treat the diffusion reaction problem within the porous structure as a one dimensional problem. A similar situation for diffusion and adsorption in nanoporous silica particles has been discussed by Amatore[37-38]. The appropriate model for one dimensional diffusion in a film coupled to complex formation and reaction has been described by Albery et al.[39-41] and was previously used in our group to describe the oxidation of NADH at polymer modified electrodes[42-44]. According to this model the current is given by

$$i = nFAK_MD_Sy/L \quad (6)$$

and

$$y=\{2\varepsilon[\alpha-\ln(1+\alpha)]\}^{1/2}\tanh\left[\frac{\varepsilon^{1/2}\alpha}{(1+\alpha)\{2[\alpha-\ln(1+\alpha)\}^{1/2}}\right] \quad (7)$$

where L is the thickness of the film, D is the diffusion coefficient of H_2O_2 in the film (assumed to be equal to the diffusion coefficient of H_2O_2 in the bulk) and

$$\varepsilon = \frac{L^2\Gamma_{site}k_{cat}}{DK_M} \quad (8)$$

and

$$\alpha = [H_2O_2]_0/K_M \quad (9)$$

where $[H_2O_2]_0$ is the concentration at the surface of the Rh film. The film thickness was estimated

from the deposition charge, Q,

$$L = \sigma Q \quad (10)$$

where σ was taken as 289 cm·C^{-1} for the 25 μm diameter electrodes.

The concentration of hydrogen peroxide at the electrode surface was calculated using

$$[H_2O_2]_0 = [H_2O_2]_{bulk} - i/nFAK'_D \quad (11)$$

where, in the case of the microdisc electrode,

$$K'_D = 4D/\pi\alpha \quad (12)$$

and we use the diffusion coefficient for hydrogen peroxide, 1.48×10^{-5} cm^2·s^{-1}, obtained above.

Eqs. (6) to (12) define four different limiting cases for the behaviour of the system. The interrelation between the four cases together with the limiting expressions for the current in each case and expressions for the current across the boundaries of the different cases are given in Fig. 7.

The four possible cases correspond to different physical situations. In Case I the film is thin ($\varepsilon < 1$) and the concentration of H_2O_2 is insufficient to saturate the reaction sites ($\alpha < 1$). As a result the reaction occurs throughout the film and the current is first order in H_2O_2 and depends on film thickness. In Case II the film is thick ($\varepsilon > 1$) but the concentration of H_2O_2 is insufficient to saturate the reaction sites ($\alpha < 1$). Under these conditions the H_2O_2 is consumed in a first order reaction layer at the outside of the film and the current is first order in H_2O_2 but independent of the film thickness. In Case III the concentration of H_2O_2 is now sufficient to saturate the sites ($\alpha > 1$) and the film is sufficiently thin ($\varepsilon < 2\alpha$) so that the reaction of H_2O_2 occurs with zero order kinetics throughout the whole film. As a result the current is independent of H_2O_2 but increases with film thickness. In Case IV the concentration of H_2O_2 is sufficient to saturate the sites at the upper part of the pore ($\alpha > 1$) but falls as it is consumed within the film ($\varepsilon > 2\alpha$) so that the kinetics become unsaturated further into the film. Under these conditions the current is half order in H_2O_2 but independent of film thickness.

3.5 Analysis of Microelectrode Results

The effect of the H$_1$e Rh film thickness on the hydrogen peroxide oxidation current was investigated to test the model described above. Fig. 8 shows the calibration data for eight different thicknesses between 45 nm and 3.56 μm over the range of 0 to 75 mmol·L^{-1} of hydrogen peroxide.

At low concentrations the current increases

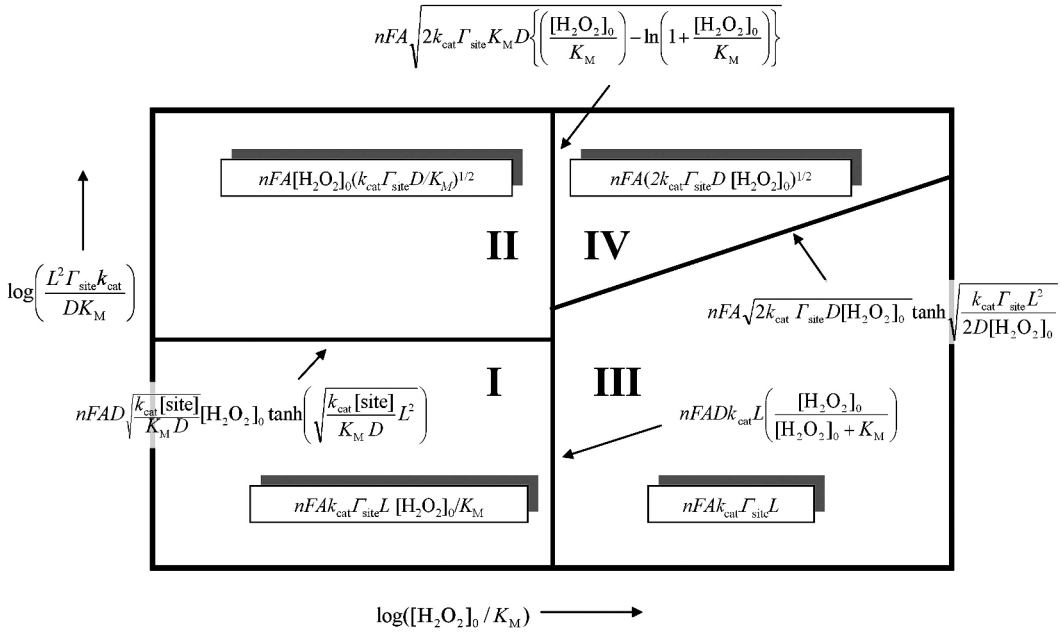

Fig. 7 The case diagram showing the four cases, the approximate analytical expressions for the current in each case and the approximate analytical expressions for the current across the boundaries between cases.

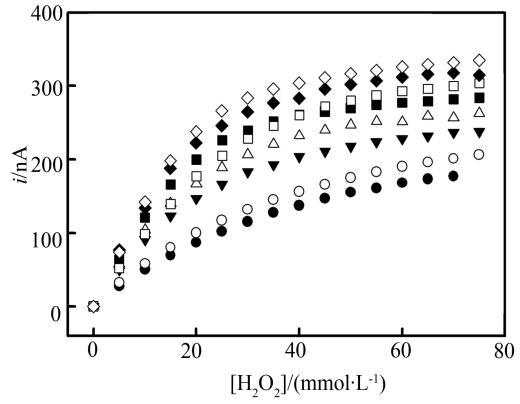

Fig. 8 Calibration curves for hydrogen peroxide oxidation obtained from chronoamperometry at 0 V vs. SMSE for H_1e Rh coated platinum microelectrodes for different Rh thicknesses in 0.1 mol·L^{-1} phosphate buffer (pH = 7, T = 25 ℃). The different thicknesses are obtained with different deposition charges: (●) 0.434, (○) 0.868, (▼) 1.74, (Δ) 5.52, (■) 8.68, (□) 17.36, (◆) 26.04, and (◇) 34.72 C. The electrode was held at 0 V vs. SMSE for 20 min before the addition of aliquots of hydrogen peroxide.

with increasing H_2O_2 and then becomes independent of H_2O_2 at high concentration (above 40 mmol·L^{-1}). According to our model, if the current is independent of H_2O_2 we should be in Case III but if this were correct the current should be proportional to the film thickness and this is clearly not the case.

There are several obvious possibilities to account for this discrepancy including possible inhibition by the product or physical blocking of the pores by oxygen gas generated in the reaction. We now consider these in turn. To test for product inhibition we investigated the current for hydrogen peroxide oxidation at an H_1e Rh coated rotating disc electrode in the presence, and in the absence, of oxygen in solution (data not shown) but found no evidence for inhibition by oxygen. To test for the possibility of blocking of the pores by oxygen gas bubbles generated by hydrogen peroxide oxidation we carried impedance measurement at 0 V vs. SMSE over the range 0.1 Hz to 100 kHz in the absence of hydrogen peroxide and whilst oxidising hydrogen peroxide at the porous electrode (data not shown). If oxygen gas is formed and blocks the pores there should be a significant change in the double layer capacitance of the electrode because of the decrease in electrochemical accessible surface area. Again we found no effect. We therefore consider next the possible effects of local changes in pH.

3.6 Effect of the Phosphate Buffer Concentration

The oxidation of hydrogen peroxide liberates protons, see Eqs. (3) to (5). In a nanoporous solid this can lead to local changes in pH if the concentration of the buffer is insufficient. This effect has been reported by Kicela and Daniele for hydrogen peroxide oxidation at platinum black electrodes [45]. If the solution at the bottom of the pores becomes acidic because of insufficient buffering, Fig. 9, this will shift the voltammetry of the Rh oxide so that the surface is no longer covered by $Rh(OH)_3$ at 0 V (see schematic voltammograms in Fig. 9) and switch off hydrogen peroxide in the bottom of the pore.

Increasing the buffer capacity will, in general, also change the ionic strength of the solution. Therefore to first test whether the current was altered by increasing the ionic strength we investigated the effect of adding K_2SO_4 while maintaining the concentration of the phosphate buffer constant. For a 'thick' mesoporous Rh film (34.72 μC deposition charge, ~ 3.6 μm thick) we observed a slight decrease (~ 10%) in the oxidation current for hydrogen peroxide on going from 0.1 mol·L^{-1} phosphate buffer to 0.1 mol·L^{-1} phosphate buffer with 0.2 mol·L^{-1} K_2SO_4 (results not shown). This can be accounted for in the slight change in the pH of the buffer solution from 7.00 to 6.83 on addition of K_2SO_4.

The effect of the buffer capacity was then investigated by changing the concentration of the phosphate buffer, Fig. 10. At low buffer capacity the current reaches a plateau at the lowest hydrogen peroxide concentration and, on increasing the buffer capacity, the response to hydrogen peroxide continues to higher concentrations. These results are consistent with hydrogen peroxide oxidation occurring further into the pore at high concentrations for higher-

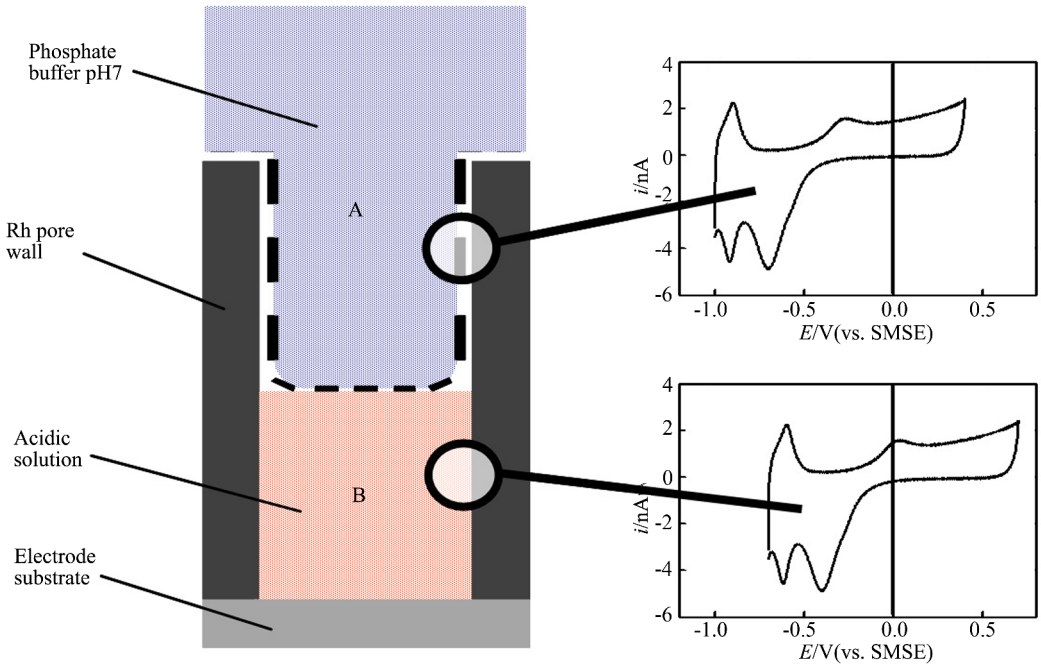

Fig. 9 Schematic representation of reaction within the pore. The dashed line represents the demarcation between the phosphate buffer (pH = 7) (A) and a more acidic solution down the pore (B). The two voltammograms on the right show the Rh electrochemistry in neutral and acidic solution and the vertical solid line marks the applied potential (0 V vs. SMSE).

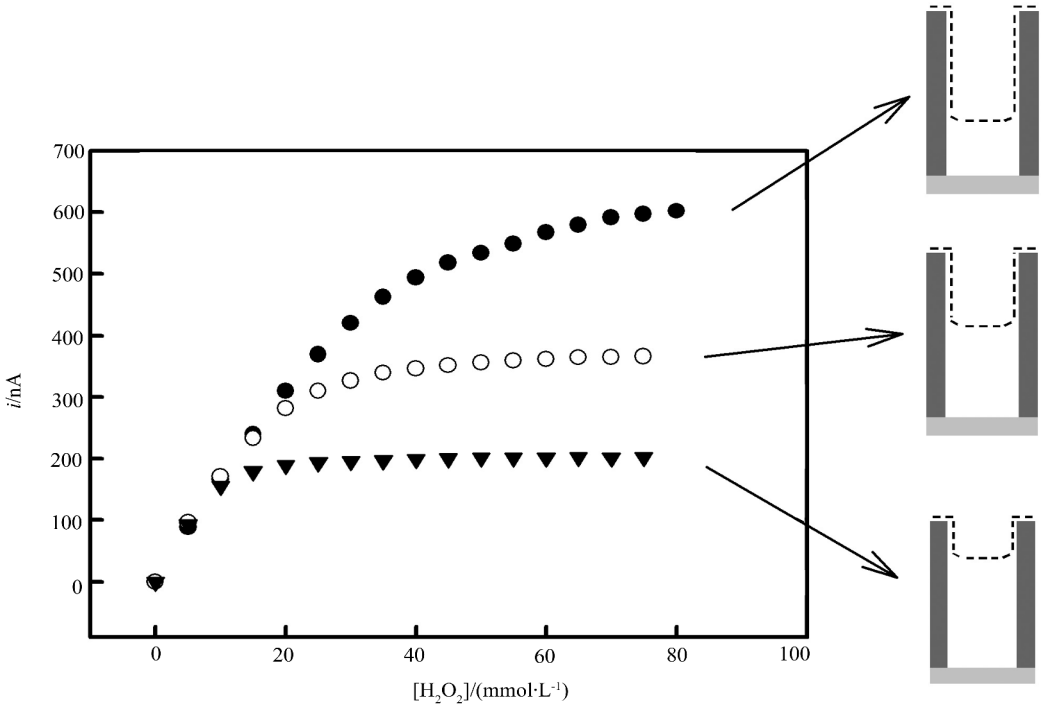

Fig. 10 Calibration curves at 0 V vs. SMSE for the oxidation of hydrogen peroxide at an H_1e Rh coated platinum microelectrode (25 μm diameter, 34.72 μC deposition charge) for different concentrations of the phosphate buffer, pH = 7, T = 25 ℃: (●) 0.2 mol·L^{-1}. (○) 0.1 mol·L^{-1}, and (▼) 0.05 mol·L^{-1}. The electrode was held at 0 V vs. SMSE for 20 min before the addition of aliquots of hydrogen peroxide. The drawings on the right indicate the approximate depth to which the hydrogen peroxide oxidation penetrates within the pore.

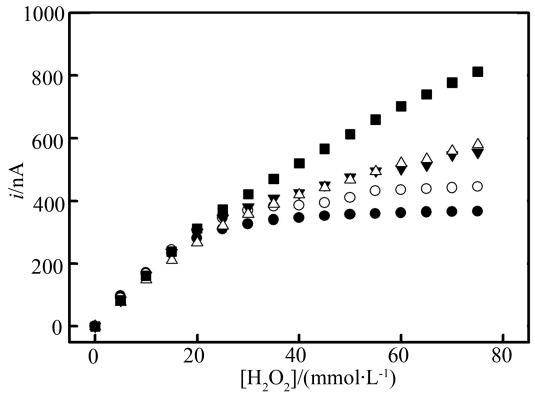

Fig. 11 Calibration curves for the oxidation of hydrogen peroxide at an H_1e Rh coated platinum microelectrode (25 μm diameter, 34.72 μC deposition charge) in 0.1 mol·L^{-1} phosphate buffer (pH = 7, T = 25 ℃) recorded at different potentials: (●) 0 V, (○) 0.05, (▼) 0.1, (Δ) 0.15, and (■) 0.2 V vs. SMSE. The electrode was held at the appropriate potential for 20 min before the addition of aliquots of hydrogen peroxide.

buffer capacity.

From Fig. 9 we can see that increasing the electrode potential should also increase the current at high concentrations of hydrogen peroxide since this will allow the $Rh(OH)_3$ to be formed at the Rh pore surface under more acidic conditions. Fig. 11 shows a set of calibration curves recorded at different potentials.

At concentrations of hydrogen peroxide up to 25 mmol·L^{-1} the currents are linear and independent of potential. At higher concentrations, when acidification within the pores starts, the oxidation currents are higher at higher potential as expected from the model.

The calibration curve obtained at 0.2 V vs. SMSE is consistent with that of Evans et al.[2] obtained at 0.6 V vs. Ag/AgCl (~ 0.2 V vs. SMSE) for an H_1e Pt coated microelectrode. The values and the trend of the calibration curve in their study are similar to our present work.

Fig. 12 shows the calibration curves and the best fits for the 'thin' H_1e Rh films to Eqs. (6) to (12) for the diffusion reaction model. The corresponding fitting parameters are given in Tab. 1. From Fig. 11 we can see that the fit to the model is good for the individual thin films and we obtain a value of ~ 20 mmol·L^{-1} for K_M with a value for $k_{cat}\Gamma_{site}\sigma$ of ~ 4 mol·cm^{-2}·C^{-1}·s^{-1} under these conditions. In this analysis we have made the simplification that the diffusion coefficient for hydrogen peroxide within the pores has the same value as the bulk. For very small pores there may be significant effects on the rate of diffusion within the pore as discussed by Amatore[37]. In the present case this would not have an effect on the analysis because we consider only the thin layer cases I and III where the diffusion coefficient within the pore does not occur in the expressions for the current.

4 Conclusions

Mesoporous Rh films were deposited onto platinum microelectrodes from the H_1 lyotropic liquid crystalline phase. These electrodes show well defined voltammetry for the oxidation and the reduction of hydrogen peroxide at low (<10 mmol·L^{-1}) concentrations with excellent stability for operation at neutral pH. From the mass transport limited current at low concentration we obtain a diffusion coef-

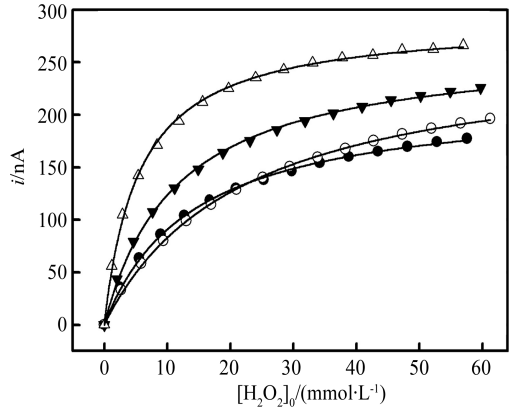

Fig. 12 Non-linear least squares fits for the hydrogen peroxide calibration curves for the thin H_1e Rh films. The H_1e Rh was deposited on a 25 μm Pt microelectrode with deposition charges of (●) 0.434, (○) 0.868, (▼) 1.74, and (Δ) 5.52 μC. All currents were recorded in 0.1 mol·L^{-1} phosphate buffer, pH = 7, T = 25 ℃ at 0 V vs. SMSE. The solid lines correspond to the best fits of the experimental curves to the expression for the case I-III boundary. The fitting parameters are given in Tab. 1.

Tab. 1 Fitting parameters for the best fits of the experimental results for thin H_1e Rh films to the expression for the case I-III boundary. The film thicknesses were estimated from Eq. (10).

Deposition charge/μC	Estimated film thickness/nm	$k_{cat}\Gamma_{site}\sigma$ /(mol·cm^{-2}·C^{-1}·s^{-1})	K_M/(mmol·L^{-1})
0.434	45	4.6±0.6	14±6.5
0.868	89	3.9±0.3	22±2.0
1.74	178	2.4±0.2	11±4.7
5.52	534	0.63±0.01	5.5±1.3

ficient for hydrogen peroxide of 1.48×10^{-5} cm^2·s^{-1} in 0.1 mol·L^{-1} pH 7 phosphate buffer.

Based on the potential dependence of the voltammetry and the hysteresis in the current we find that the oxidation of hydrogen peroxide occurs on the $Rh(OH)_3$ coated surface of the porous Rh and occurs through a CEE mechanism of the type proposed for the reaction on Pt.

At higher hydrogen peroxide concentrations, above 20 mmol·L^{-1}, the current at 0 V vs. SMSE reaches a plateau due to either saturation of the binding sites for hydrogen peroxide within the pore (for films less than ~ 100 nm thick) or limitation of the reaction of hydrogen peroxide down the pore due to acidification of the solution at the bottom of the pore.

For the thin films we were able to fit the results to a one dimensional model for diffusion and reaction within the pores. For thick films the linearity of the current response and high concentrations of hydrogen peroxide can be improved by increasing the buffer concentration or increasing the potential.

H_1e coated Rh microelectrodes show good promise for biosensor applications as they allow measurement of concentrations of hydrogen peroxide at several mmol·L^{-1} and below in pH 7 solution at lower overpotentials (around 0.4 vs. SCE) than Pt with excellent stability.

Acknowledgments

This work was supported by the EPSRC Grant EP/E0473X/1.

Supporting Information Available:

The supporting information is available free of charge via the internet at http://electrochem.xmu.edu.cn

References:

[1] Attard G S, Bartlett P N, Coleman N R B, et al. Mesoporous platinum films from lyotropic liquid crystalline phases[J]. Science, 1997, 278(5339): 838-840.

[2] Evans S A G, Elliott J M, Andrews L M, et al. Detection of hydrogen peroxide at mesoporous platinum microelectrodes[J]. Analytical Chemistry, 2002, 74(6): 1322-1326.

[3] Chen W, Cai S, Ren Q Q, et al. Recent advances in electrochemical sensing for hydrogen peroxide: A review[J]. Analyst, 2012, 137(1): 49-58.

[4] Welch C M, Banks C E, Simm A O, et al. Silver nanoparticle assemblies supported on glassy-carbon electrodes for the electro-analytical detection of hydrogen peroxide[J]. Analytical and Bioanalytical Chemistry, 2005, 382 (1): 12-21.

[5] Prodromidis M I, Karayannis M I. Enzyme based amperometric biosensors for food analysis[J]. Electroanalysis, 2002, 14(4): 241-261.

[6] Li X Z, Liu H S. Development of an E-H_2O_2 /TiO_2 photoelectrocatalytic oxidation system for water and wastewater treatment[J]. Environmental Science & Technology, 2005, 39(12): 4614-4620.

[7] Armstrong F A, Wilson G S. Recent developments in faradaic bioelectrochemistry[J]. Electrochimica Acta, 2000, 45(15/16): 2623-2645.

[8] Nowall W B, Kuhr W G. Detection of hydrogen peroxide and other molecules of biological importance at an electrocatalytic surface on a carbon fiber microelectrode[J]. Electroanalysis, 1997, 9(2): 102-109.

[9] Aoki K, Ishida M, Tokuda K, et al. Electrode-kinetics of the oxidation of hydrogen peroxide at pretreated glassy carbon and carbon fiber electrodes[J]. Journal of Electroanalytical Chemistry, 1988, 251(1): 63-71.

[10] Prabhu V G, Zarapkar L R, Dhaneshwar R G. Electrochemical studies of hydrogen peroxide at a platinum disc electrode[J]. Electrochimica Acta, 1981, 26(6): 725-729.

[11] Liu H Y, Ying T L, Sun K, et al. Reagentless amperometric biosensors highly sensitive to hydrogen peroxide, glucose and lactose based on N-methyl phenazine methosulfate incorporated in a Nafion film as an electron transfer mediator between horseradish peroxidase and an electrode[J]. Analytica Chimica Acta, 1997, 344(3): 187-199.

[12] Horrocks B R, Schmidtke D, Heller A, et al. Scanning electrochemical microscopy. 24. Enzyme ultramicroelectrodes for the measurement of hydrogen peroxide at surfaces[J]. Analytical Chemistry, 1993, 65(24): 3605-3614.

[13] Ruzgas T, Csoregi E, Emneus J, et al. Peroxidase-modified electrodes: Fundamentals and application[J]. Analytica Chimica Acta, 1996, 330(2/3): 123-138.

[14] Karyakin A A. Prussian Blue and its analogues: Electrochemistry and analytical applications[J]. Electroanalysis, 2001, 13(10): 813-819.

[15] E. N. K. Wallace, in PhD thesis, University of Southampton, 1997.

[16] D. A. Cook, in PhD thesis, University of Southampton, 2005.

[17] Zhang Y, Wilson G S. Electrochemical oxidation of H_2O_2 on Pt and Pt + Ir electrodes in physiological buffer and its applicability to H_2O_2-based biosensors[J]. Journal of Electroanalytical Chemistry, 1993, 345(1/2): 253-271.

[18] Gorton L. A carbon electrode sputtered with palladium and gold for the amperometric detection of hydrogen peroxide[J]. Analytica Chimica Acta, 1985, 178(2): 247-253.

[19] Johnston D A, Cardosi M F, Vaughan D H. The electrochemistry of hydrogen peroxide on evaporated gold/palladium composite electrodes—manufacture and chemical characterization[J]. Electroanalysis, 1995, 7(6): 520-526.

[20] Hall S B, Khudaish E A, Hart A L. Electrochemical oxidation of hydrogen peroxide at platinum electrodes. Part 1. An adsorption-controlled mechanism[J]. Electrochimica Acta, 1998, 43(5/6): 579-588.

[21] Hall S B, Khudaish E A, Hart A L. Electrochemical oxidation of hydrogen peroxide at platinum electrodes. Part II: Effect of potential[J]. Electrochimica Acta, 1998, 43(14/15): 2015-2024.

[22] Hall S B, Khudaish E A, Hart A L. Electrochemical oxidation of hydrogen peroxide at platinum electrodes. Part III: Effect of temperature[J]. Electrochimica Acta, 1999, 44(14): 2455-2462.

[23] Hall S B, Khudaish E A, Hart A L. Electrochemical oxidation of hydrogen peroxide at platinum electrodes. Part IV: Phosphate buffer dependence[J]. Electrochimica Acta, 1999, 44(25): 4573-4582.

[24] Hall S B, Khudaish E A, Hart A L. Electrochemical oxidation of hydrogen peroxide at platinum electrodes. Part V: Inhibition by chloride[J]. Electrochimica Acta, 2000, 45(21): 3573-3579.

[25] Elliott J M, Birkin P R, Bartlett P N, et al. Platinum microelectrodes with unique high surface areas[J]. Langmuir, 1999, 15(22): 7411-7415.

[26] Han J H, Boo H, Park S, et al. Electrochemical oxidation of hydrogen peroxide at nanoporous platinum electrodes and the application to glutamate microsensor[J]. Electrochimica Acta, 2006, 52(4): 1788-1791.

[27] Miscoria S A, Barrera G D, Rivas G A. Glucose biosensors based on the immobilization of glucose oxidase and polytyramine on rhodinized glassy carbon and screen printed electrodes[J]. Sensors and Actuators B-Chemical, 2006, 115(1): 205-211.

[28] Rodríguez M C, Rivas G A. An enzymatic glucose biosensor based on the codeposition of rhodium, iridium, and glucose oxidase onto a glassy carbon transducer[J]. Analytical Letters, 2001, 34(11): 1829-1840.

[29] Bartlett P N, Marwan J. Preparation and characterization of H_1e rhodium films[J]. Microporous and Mesoporous Materials, 2003, 62(1/2): 73-79.

[30] Vogel A I, Bassett J. Vogel's textbook of quantitative inorganic analysis: Including elementary instrumental analysis[M]. English Language Book Society, 1986.

[31] Jerkiewicz G, Borodzinski J J. Studies of formation of very thin oxide-films on polycrystalline rhodium electrodes—application of the Mott-Cabrera theory[J]. Langmuir, 1993, 9(8): 2202-2209.

[32] Jerkiewicz G, Borodzinski J J. Relation between the sur-

face-states of oxide-films at Rh electrodes and kinetics of the oxygen evolution reaction[J]. Journal of The Chemical Society-Faraday Transactions, 1994, 90(24): 3669-3675.

[33] Peuckert M. A comparison of the thermally and electrochemically prepared oxidation adlayers on rhodium—chemical nature and thermal stability[J]. Surface Science, 1984, 141(2/3), 500-514.

[34] Florit M I, Bolzan A E, Arvia A J. Reactions involving H, OH and O species on rhodium in $H_2SO_4 \cdot 12H_2O$ and $HClO_4 \cdot 5.5H_2O$ in the range 198-298 K[J]. Journal of Electroanalytical Chemistry, 1995, 394(1/2): 253-262.

[35] Katsounaros I, Schneider W B, Meier J C, et al. Hydrogen peroxide electrochemistry on platinum: Towards understanding the oxygen reduction reaction mechanism [J]. Physical Chemistry Chemical Physics, 2012, 14(20): 7384-7391.

[36] Vanstroebiezen S A M, Everaerts F M, Janssen L J J, et al. Diffusion coefficients of oxygen, hydrogen peroxide and glucose in a hydrogel[J]. Analytica Chimica Acta, 1993, 273(1/2): 553-560.

[37] Amatore C. Theoretical trends of diffusion and reaction into tubular nano- and mesoporous structures: General physicochemical and physicomathematical modeling[J]. Chemistry-A European Journal, 2008, 14(18): 5449-5464.

[38] Amatore C, Oleinick A, Klymenko O V, et al. Theory and simulation of diffusion-reaction into nano- and mesoporous structures. Experimental application to sequestration of mercury (II) [J]. Analytical Chemistry, 2008, 80(9): 3229-3243.

[39] Albery W J, Cass A E G, Shu Z X. Inhibited enzyme electrodes. 1. Theoretical model[J]. Biosensors & Bioelectronics, 1990, 5(5): 367-378.

[40] Albery W J, Cass A E G, Shu Z X. Inhibited enzyme electrodes.2. The kinetics of the cytochrome-oxidase system[J]. Biosensors & Bioelectronics, 1990, 5 (5): 379-395.

[41] Albery W J, Cass A E G, Mangold B P, et al. Inhibited enzyme electrodes. 3. A sensor for low-levels of H_2S and HCN[J]. Biosensors & Bioelectronics, 1990, 5 (5): 397-413.

[42] Bartlett P N, Birkin P R, Wallace E N K. Oxidation of β-nicotinamide adenine dinucleotide (NADH) at poly (aniline)-coated electrodes[J]. Journal of the Chemical Society-Faraday Transactions, 1997, 93(10): 1951-1960.

[43] Bartlett P N, Simon E. Poly(aniline)-poly(acrylate) composite films as modified electrodes for the oxidation of NADH[J]. Physical Chemistry Chemical Physics, 2000, 2(11): 2599-2606.

[44] Bartlett P N, Wallace E N K. The oxidation of β-nicotinamide adenine dinucleotide (NADH) at poly(aniline) -coated electrodes Part II. Kinetics of reaction at poly (aniline)-poly (styrenesulfonate) composites [J]. Journal of Electroanalytical Chemistry, 2000, 486(1): 23-31.

[45] Kicela A, Daniele S. Platinum black coated microdisk electrodes for the determination of high concentrations of hydrogen peroxide in phosphate buffer solutions[J]. Talanta, 2006, 68(5): 1632-1639.

H_2O_2 在具有纳米结构的 Rh 微电极上的电催化氧化

Philip N. Bartlett*, Thomas F. Esterle
(南安普顿大学化学系, 英国 南安普顿 SO17 1BJ)

摘要： 在含有 $C_{12}EO_8$(Octaethyleneglycol Monododecyl Ether)的 H_1 溶致液晶相中 Pt 微电极上电沉积 Rh 介孔膜. 该电极在中性、低浓度(CH_2O_2<10 mmol·L^{-1})条件下,对 H_2O_2 有较好的氧化还原响应及稳定性. 由于电流磁滞效应,H_2O_2 在 Rh 介孔膜微电极上的氧化与电位相关,且遵循与 $Rh(OH)_3$ 有关的 CEE(Chemical reaction step by two sequential electrochemical steps)反应机制. H_2O_2 浓度较大时,由于孔电极表面其结合点位趋于饱和或孔内溶液酸化的反应限制，电流呈现一平台. Rh 介孔膜厚度小于 200 nm 的电极,H_2O_2 浓度校正曲线符合膜孔反应一维扩散模型.

关键词： H_2O_2; Rh; 微电极; 纳米孔; 溶致液晶; 模板电沉积